

# A Detection Scheme for Integrated SWIPT Receivers with Rectenna Arrays

Eleni Goudeli, *Graduate Student Member, IEEE*, Constantinos Psomas, *Senior Member, IEEE*,  
and Ioannis Krikidis, *Fellow, IEEE*

**Abstract**—Smart devices and their applications led to a rapid evolution of the Internet of Things. As a result, there is an emerging need on energizing those low-power devices, while at the same time achieving information transfer. In this context, simultaneous wireless information and power transfer (SWIPT) is considered as an appealing technology, since it can power wirelessly and remotely such devices, simultaneously with information transfer. Motivated by this, we herein propose a system model with an integrated SWIPT receiver, succeeding enhanced performance in terms of information decoding (ID) and energy harvested (EH). Specifically, we adopt a single input multiple output topology, where at the receiver's side we examine two antenna architectures, one based on the direct-current (DC) combining and the other on the radio-frequency (RF) combining. For both schemes, we consider multiple receive antennas and rectifiers, comparing their performances. Furthermore, we adopt a piece-wise linear EH model, which takes into account the sensitivity and saturation effects of the rectifiers. By using a maximum likelihood-based soft decoding, a non-coherent energy detection is achieved. Finally, an asymptotic analysis is conducted, providing upper and lower bounds for ID and EH, respectively. Simulation results along with theoretical analysis, validate the enhanced performance both in terms of ID and EH.

**Keywords**—SWIPT, integrated receiver, piece-wise linear energy harvesting, non-coherent detection, maximum likelihood-based soft decoding.

## I. INTRODUCTION

In the new era of the Internet of Things (IoT) and wireless sensor networks, wireless power transfer (WPT) has been recognized as a promising technology to overcome the critical challenge of supplying power, remotely and wirelessly, to an extensive number of low-power IoT devices [2]. Specifically, radio-frequency (RF) signals are considered as a viable source for WPT, since they have the ability to energize devices over a long distance. On the other hand, RF signals have been widely used for wireless information transmission. Therefore, a simultaneous wireless information and power transfer (SWIPT) system, where RF signals simultaneously convey data and energy, is considered an appealing solution for networks with low-power devices [3]. Some challenges that may provide a practical limitation to SWIPT receivers are distance constraints, energy harvesting (EH) efficiency,

maintaining field strength within safety limits, use of a high frequency for energy transmission and mobility of the sensor nodes [4].

Nonetheless, SWIPT has attracted significant interests in the communication literature. Considering that the rectifying process from RF to direct current (DC) is similar to an envelope detection process, there are numerous studies, in order to achieve enhanced performance for simultaneous power and information transfer. Therefore, from the rectified signal at the receiver, several different parameters are detected and exploited. In particular, the authors in [5] study the intermodulation of multi-frequency transmission signal by exploiting both the amplitude and the phase. In [6], a pulse position modulation, where information is encoded in the position of the pulse, is investigated. Finally, in [7] and [8], information decoding (ID) is achieved by detecting the power variations in the received signal adopting a tone-index multisine modulation or enhanced biased amplitude-shift keying, respectively. In the same context, this paper focuses on how the rectified signal may succeed enhanced ID performance, by exploiting the architecture of the receiver at a basic SWIPT system.

A SWIPT system has two fundamental architectures [9] regarding the receiver. In the first one, the received RF signal is split into two parts, either in the time or in the power domain. One part of the RF signal, is used for information transfer and another part for EH. In the second architecture, an integrated ID and EH circuit is adopted. Specifically, the received RF signal is channeled to a rectifier and a low-pass filter, thus converted to DC signal. Afterwards, the DC power signal is split into two parts for ID and EH, respectively. Therefore, the baseband conversion is replaced by a rectification circuit. The idea was introduced in [10], where the rate-energy tradeoff for a point-to-point system was investigated. A considerable benefit of the integrated architecture, is that by replacing the active RF to baseband conversion with a passive rectifier operation, it can significantly reduce the power consumption of a SWIPT receiver. As such, considering low-power IoT solutions, we herein adopt the architecture of the integrated SWIPT receiver.

Furthermore, targeting enhanced performance for ID and EH, we herein examine two different topologies, with multiple antennas and rectifiers at the receiver's side. In the state-of-the-art, multiple antenna system models are traditionally considered as a common solution for enhanced performance either in terms of ID or EH. There are various studies conducted for exclusively EH technologies, trying to overcome the need of providing enough energy for a reliable EH operation

Preliminary results of this work will be presented at the IEEE Vehicular Technology Conference, Helsinki, Finland, 2022 [1].

This work has received funding from the European Research Council (ERC) under the European Union's Horizon 2020 research and innovation programme (Grant agreement No. 819819). It was also co-funded by the European Regional Development Fund and the Republic of Cyprus through the Research and Innovation Foundation, under the project INFRASTRUCTURES/1216/0017 (IRIDA).

[11], [12]. In addition, in the communication and signal processing literature, it is proven that multiple antenna systems demonstrate a great improvement of performance in terms of spectral efficiency and higher data rates, succeeding diversity or multiplexing gains [13]-[15]. Same-wise, SWIPT has also been an area of research for attracting interest on multiple antennas. Specifically, in [16] the authors study a two-way relay system with multiple users and a multi-antenna relay employing SWIPT strategy, where splitting the received signal leads to a rate-energy trade-off. In [17], authors investigate SWIPT with a multi-antenna transmitter sending data and energy to single antenna receivers adopting a time switching circuit. Beamforming for energy transfer and information transmission is considered in [18], achieving the maximal energy efficiency.

In addition, we focus our interest on the rectenna architectures that are usually investigated. Specifically, there are two basic schemes in the literature: i) DC combining, where each antenna branch incorporates its own rectifier to separately harvest power, and ii) RF combining, where all the antennas are arranged to channel the RF power to a single rectifier [19]. In DC combining, the rectifiers must individually rectify low RF powers, resulting in low conversion efficiency [20]. On the other hand, RF combining channels the combined signal to a single rectifier, which therefore operates on higher input power levels and achieves higher conversion efficiencies [21]. As such, while the DC combining scheme in most cases surpasses the RF combining scheme, there are operation scenarios where RF scheme is superior. Furthermore, there are also some studies trying to succeed a hybrid solution [12]. The authors in [22], adopt the beamforming matrix in a hybrid power combining rectenna array. While, in [23] authors consider a single-input multiple-output (SIMO) topology where each receive antenna is connected to multiple rectifiers. We herein, adopt this technique, studying both DC and RF combining schemes, differentiating this way from the conventional rectennas solutions.

At the same time, we take into consideration an important area of SWIPT, that the vast majority of research in the RF literature has been devoted to. Specifically, we refer to the design of efficient energy harvesters, so as to increase the RF-to-DC conversion efficiency [25]-[27]. The appropriate choice of models in order to describe the input-output characteristic of a rectenna, is another challenge in the SWIPT technology. Earlier works on SWIPT have been characterized under simplifying assumptions for the rectenna models. Targeting the most realistic approach several models have been proposed, driven by a tradeoff between accuracy and tractability [28]. It has been shown, that linear models do not take explicitly into account the effects of rectifier's important characteristics, such as the fact that the RF-to-DC conversion efficiency is a non-linear function of its input signal shape and power. Thus, non-linear EH models are considered as an appropriate choice for a realistic approach. In our study, we adopt a piece-wise linear model [29], which although simple, approximates with accuracy the performance of the RF EH model.

Finally, regarding the ID, since RF to DC rectifying process is similar to envelope detection, we apply non-coherent energy

detection technique, where the use of channel state information (CSI) is not required [30]. For the detection of the received signals, there are plenty of mechanisms proposed in the literature. The differences depend on the architecture applied and the modulation scheme adopted. More specifically, in [31] a SWIPT solution with the use of integrated receiver and precoding on the energy patterns is presented. However, such a solution relies on the availability of CSI at the receiver, resulting in a coherent decoding scheme. Coherent techniques are a challenging task, since the source needs to periodically send training symbols, which results in increased signaling overhead and processing burden [32]. On the other hand, with the use of non-coherent techniques, such as the one that we adopt, the receiver's complexity is reduced. Specifically, we succeed this with the use of a maximum likelihood-based (ML-based) soft decoder. At the same time, in order to assure low power consumption and modest complexity, a straightforward choice for the modulation scheme, that we also adopt, is binary on-off keying (OOK) [33], [34], which can also serve as a guideline for other modulation schemes.

Overall, in this work we study SWIPT and we address the critical issue of enhanced performance in terms of ID and EH, simultaneously. In contrast to the aforementioned works, we adopt an integrated SWIPT receiver architecture, thus avoiding the RF to baseband conversion, while at the same time exploiting the received rectified DC power signal, both for ID and EH. Differentiating from the traditional rectennas, we adopt multiple receive antennas  $N$ , while connecting each one of them to multiple rectifiers,  $K$ . By exploiting two different combining schemes at the receiver's side, one in the DC domain and the other in the RF domain, we study the systems' performance, providing enhanced results both in terms of ID and EH. At the same time, we investigate and analyze the effects from the variations of sensitivity and saturation characteristics of rectifiers. Finally, with the use of ML-based soft decoding, we succeed energy detection without the use of CSI [35]. It has to be noticed that our proposed integrated SWIPT receiver with rectenna arrays, could be applied to numerous IoT applications [36], like wearable or implantable devices, radio frequency identification (RFID) bags, wireless sensor nodes etc. [37]. The main contributions of our study are as follows:

- We show that DC combining scheme surpasses the RF combining, in terms of ID. Though, it has to be noticed that the decoding complexity in the DC combining scheme is exponentially increasing with the number of receive antennas,  $(2K+1)^N$ , while in the RF combining scheme is proportional to the number of rectifiers, which is equal to  $2K+1$ . On the other hand, the RF combining scheme is superior to the DC, regarding the EH, specifically when referring to low power regime. Furthermore, as the number of antennas and rectifiers increases, the performance is enhanced for both schemes in terms of ID and EH as expected.
- In addition, by considering some special cases of the proposed schemes, we explore the system behavior. Specifically, for the simple case of multiple antennas and

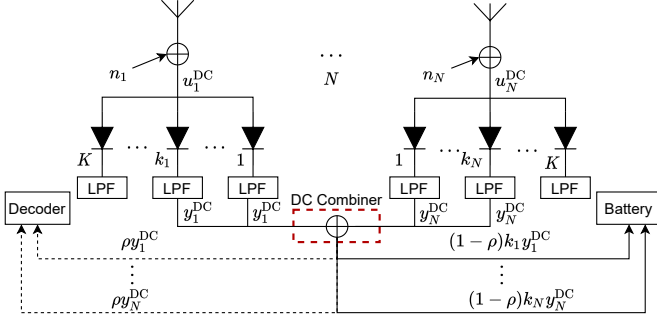


Fig. 1. Integrated SWIPT receiver, with  $N$  receive antennas and  $K$  rectifiers, DC combining.

only one rectifier, i.e.  $N, K = 1$ , it is shown that DC combining scheme lags behind in terms of symbol error rate (SER) for ID, compared to RF combining. This is specifically referring to low ranges of average transmitted power, while it is eliminated as the average transmitted power increases.

- Furthermore, comparing the case of one receive antenna with multiple rectifiers, i.e.  $N = 1, K$ , towards the case of multiple antennas with one rectifier i.e.  $N, K = 1$ , we show that the increase in the number of antennas enhances more the system performance in terms of EH, compared to the increase of the rectifiers, both for DC and RF combining scheme. The same applies for the performance of the ID in terms of SER, for low ranges of  $P$ . Though, as the average transmitted power increases the two schemes differentiate. Specifically, in DC combining the performance is the same, either if we increase  $N$  or  $K$ , while for the RF scheme the performance is bounded by the number of rectifiers.
- Finally, we present numerical results that validate our analysis, while we examine the behavior of our proposed solutions as the sensitivity and saturation levels variate. It is interesting that in low power regime, the RF combining scheme surpasses the DC scheme in terms of ID even for high saturation levels. Furthermore, in RF scheme the variations on the sensitivity and saturation levels do not affect so intensively the SER performance compared to the DC scheme. An asymptotic analysis in high average transmitted power regime is carried out, providing upper and lower bounds for ID and EH, respectively.

The rest of the paper is organized as follows. Section II presents the system model and our main assumptions. Section III provides the analytical framework for the derivation of SER, while Section IV of average EH. In Section V, we asymptotically examine the behavior of the proposed system models. Finally, Section VI presents the numerical results and Section VII concludes our work.

**Notation:** Lowercase boldface letters denote vectors;  $\mathbb{P}(X)$  denotes the probability of the event  $X$ , while  $\mathbb{E}[X]$  represents the expected value of  $X$ ;  $f(y)$  denotes the probability density function of  $y$  and  $\binom{\alpha}{\beta} = \frac{\alpha!}{\beta!(\alpha-\beta)!}$  denotes the binomial coefficient. Furthermore,  $F_y(\cdot)$  and  $\bar{F}_y(\cdot)$  denote the cumulative and complementary cumulative density function of  $y$ . Finally,  $\lceil \cdot \rceil$

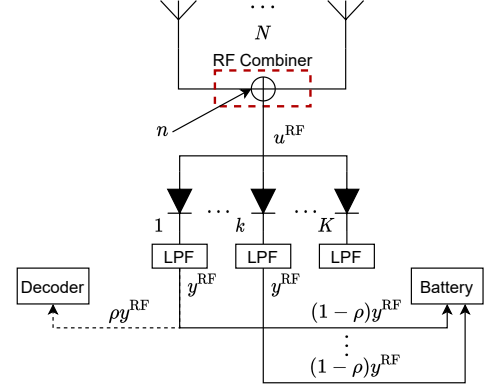


Fig. 2. Integrated SWIPT receiver, with  $N$  receive antennas and  $K$  rectifiers, RF combining.

is the ceiling operator,  $\delta(x)$  denotes the Dirac delta function, while the main mathematical notation used in the paper is summarized in Table I.

## II. SYSTEM MODEL

### A. Integrated Receiver Architecture

We consider a SWIPT system, with a single antenna transmitter at the source, that transmits a baseband signal  $x(t)$  with  $\mathbb{E}[|x(t)|^2] = 1$ . Symbols  $x \in [0, 1]$  are transmitted with equal probability. It is herein noted, that the derivations of our analysis could be extended to other modulation schemes suitable for energy detection such as pulse energy modulation (PEM) [31]. On the contrary, we herein note that conventional bipolar pulse-amplitude modulation (BPAM) can not be readily used, since transmitted symbols convey the same energy and therefore cannot be distinguished by the integrated receiver.

The baseband signal is then up-converted to generate an RF signal, which is transmitted over a Rayleigh fading channel, with a transmitted power  $P$ . At the receiver's side we adopt an integrated SWIPT receiver [10], which consists of multiple receive antennas and rectifiers,  $N$  and  $K$ , respectively.

The first topology, as seen in Fig. 1, proposes a solution with the use of a DC combiner [38]. Specifically, each receive antenna  $i \in [1, N]$  is connected to  $K$  rectifiers. Therefore, the received RF power signal at each antenna  $i$  is calculated as

$$u_i^{\text{DC}} = |\sqrt{P}h_i x + n_i|^2, \quad (1)$$

where  $h_i$  is the channel coefficient at the  $i$ -th antenna, which is modeled as a complex Gaussian random variable with zero mean and unit variance. Furthermore,  $n_i$  models the noise as an additive white Gaussian noise (AWGN) with unit variance. From (1), we notice that the received RF power signal is exponentially distributed with pdf

$$f(u_i^{\text{DC}}) = \lambda_x^{\text{DC}} e^{-\lambda_x^{\text{DC}} u_i^{\text{DC}}}, \quad (2)$$

where  $\lambda_x^{\text{DC}}$  denotes the rate parameter and is calculated from

$$\lambda_x^{\text{DC}} = 1/\mathbb{E}(u_i^{\text{DC}}) = 1/(Px^2 + 1). \quad (3)$$

TABLE I  
SUMMARY OF NOTATION

Notation	Description	Notation	Description
$N$	Total number of antennas at the receiver	$P$	Average transmitted power
$K$	Number of activated rectifiers at antenna $i$	$x$	OOK symbol
$k_i/k \in [1, K]$	Number of activated rectifiers at DC/RF scheme	$h_i$	Channel coefficient of antenna $i$
$u_{\min}$	Sensitivity power level	$n_i$	Additive white Gaussian noise to antenna $i$
$u_{\max}$	Saturation power level	$u_i^{\text{DC}}/u^{\text{RF}}$	Received power signal for DC/RF scheme
$N_{\text{sen}}$	Number of antennas in the sensitivity area	$y(u_i^{\text{DC}})/y(u^{\text{RF}})$	Output from $k_i/k$ activated rectifier at DC/RF scheme
$\alpha$	Conversion efficiency from RF to DC	$\rho$	Split power ratio for ID
$N_L$	Number of antennas in the linear area	$f(u_i^{\text{DC}})/f(u^{\text{RF}})$	Probability density function of $u_i^{\text{DC}}/u^{\text{RF}}$
$N_{\text{sat1}}$	Number of antennas in the saturation area	$\lambda_x^{\text{DC}}/\lambda_x^{\text{RF}}$	Rate parameter of exponentially distributed $u_i^{\text{DC}}/u^{\text{RF}}$
$N_{\text{sat2}}$	Number of antennas in the saturation area for $s_i = K$	$z$	Sum of $u_{l_i}$ 's
$L$	Set of antennas in linear area with $l_i \in [1, K]$	$C_m$	Combinations of antennas based on their ordering
$S$	Set of antennas in saturation area with $s_i \in [1, K-1]$	$M$	Number of tuples whose sum equals to $N$

As such we herein define  $\lambda_0^{\text{DC}} = 1$  and  $\lambda_1^{\text{DC}} = 1/(P+1)$ , that are used throughout the paper.

The second topology, as seen in Fig. 2, proposes a solution with the use of an RF combiner [39]. We still consider a SIMO solution with an integrated SWIPT receiver. Similarly, we assume  $N$  receive antennas, while the difference is that the received signals are combined in the RF domain and not in the DC. Specifically, the received RF signals from the  $N$  antennas are summed with the use of an RF combiner and then channeled to  $K$  rectifiers. The relative power signal is calculated as

$$u^{\text{RF}} = \left| \sqrt{P} \sum_{i=1}^N h_i x + n \right|^2, \quad (4)$$

where  $n$  models the AWGN with unit variance. From (4), we notice that the received power signal  $u^{\text{RF}}$  is exponentially distributed with pdf

$$f(u^{\text{RF}}) = \lambda_x^{\text{RF}} e^{-\lambda_x^{\text{RF}} u^{\text{RF}}}, \quad (5)$$

where  $\lambda_x^{\text{RF}}$  denotes the rate parameter and is calculated from

$$\lambda_x^{\text{RF}} = 1/\mathbb{E}(u^{\text{RF}}) = 1/(PNx^2 + 1). \quad (6)$$

As such we herein define  $\lambda_0^{\text{RF}} = 1$  and  $\lambda_1^{\text{RF}} = 1/(PN+1)$ .

### B. RF-to-DC Rectenna Model

For both proposed topologies, we assume that all the rectifiers exhibit the same characteristics. Specifically, we consider two power levels,  $u_{\min}$  and  $u_{\max}$ , that denote the sensitivity and saturation level of each rectifier, respectively. In case the RF power signal channeled to a rectifier is less than  $u_{\min}$ , then the rectification circuit is not activated. On the other hand, if it is higher than  $u_{\max}$ , then it reaches the saturation area, where the DC output is maximized. Over the interval  $u_{\min}$  and  $u_{\max}$ , the activated rectifier is in the linear region, where the DC output is linearly increased with the input power. The model adopted, in order to describe the above non-linearity between the RF power signal and the DC output, is the constant-linear-constant (CLC) model [29].

With the use of multiple rectifiers, for both proposed schemes, we target to enhance the output DC signal. Specifically, by taking into consideration the proposed solution in Fig. 1, the received RF signal at each antenna  $i$ ,  $u_i^{\text{DC}}$ , is led to the

$K$  rectifiers. Depending on the power of the received signal, an optimum number of rectifiers,  $k_i$ , is activated, thus overcoming the saturation effect and harvesting more energy, compared to a single rectenna solution. Based on the CLC model adopted, the DC output might be in the sensitivity, linear or saturation area, and is calculated respectively as

$$y_i^{\text{DC}} = 0, \quad (7)$$

$$y_i^{\text{DC}} = \alpha \left( \frac{u_i^{\text{DC}}}{k_i} - u_{\min} \right), \quad (8)$$

$$y_i^{\text{DC}} = y_{\text{sat}}, \quad (9)$$

where parameter  $\alpha$  denotes the conversion efficiency and ranges between  $(0, 1]$ , while  $y_{\text{sat}} = \alpha(u_{\max} - u_{\min})$ .

Following the same steps as described above and by considering the second proposed solution with the RF combiner, Fig. 2, we calculate accordingly the relevant DC output. Specifically, we denote it as  $y^{\text{RF}}$  and is given from (7), (8) and (9), by substituting the received power signal  $u_i^{\text{DC}}$  with  $u^{\text{RF}}$ , as calculated in (4). Finally, for this scheme we denote the activated rectifiers with  $k \in [0, 1]$ .

### C. Decoding Model

In the conventional SWIPT architecture schemes, the received RF signal is firstly split into the power or time domain and then channeled for ID and EH. On the contrary, in the integrated SWIPT architecture that we adopt, the received signal is fully converted from RF to DC and then split into two streams for ID and EH. Specifically, the split power ratio is  $\rho$  for ID and  $1 - \rho$  for EH. Furthermore, in order to reduce the energy requirements for the symbol detection and jointly maximize the power split for EH, we consider that  $\rho \rightarrow 0$  [10]. As such, since it takes an infinitely small value, we do not consider it in the analysis of SER and EH in Section III, Section IV, and Section VI.

1) *DC Combiner*: As seen in Fig. 1, the DC outputs from the activated rectifiers at each antenna  $i$ , i.e.  $k_i y_i^{\text{DC}}$ , are channeled to the DC combiner. Afterwards, the decoder in order to optimally combine and decide on the transmitted symbol  $x$ , samples a small portion of the DC output from one activated rectifier at each antenna  $i$ , i.e.  $\rho y_i^{\text{DC}}$ . This is due to the fact that the received RF signal at each antenna  $i$  is equally

split to the rectifiers, which exhibit the same characteristics. Therefore, the  $k_i$  DC outputs from an antenna  $i$  are identical. At the same time, the battery is charged with the remaining DC outputs from all the activated rectifiers  $k_i$ , at each antenna  $i$ , i.e.  $\sum_{i=1}^N (1 - \rho) k_i y_i^{\text{DC}}$ .

The optimum decision of the decoder is based on energy detection, avoiding the knowledge of CSI and is calculated with the use of a ML-based soft decoder. In contrary to a hard decision decoder, the optimum decision is taken by considering the DC outputs from all  $N$  antennas and finally deciding based on the overall maximum likelihood of the transmitted symbol  $x$ . On the other hand, with the use of a hard decoder, the decision on the transmitted symbol is estimated independently, with the use of ML, at the output of each antenna and the final decision rule is based on the majority of estimated symbols  $\tilde{x}$ .

Therefore, in this paper the optimum decision rule, which is calculated with the use of a ML-based soft decoder, is based on the observation vector  $\mathbf{y}^{\text{DC}}$  and the symbol that yields the maximum conditioned density  $f(\mathbf{y}|x)$  is selected

$$\tilde{x} = \arg \max_{x \in \{0,1\}} f(\mathbf{y}|x), \quad (10)$$

where  $\mathbf{y}$  is a  $N \times 1$  vector, denoting the DC outputs from all the  $N$  receive antennas, given that  $x$  is transmitted. Since noise is independent between different receive antennas, the distribution  $f(\mathbf{y}|x)$  can be factored like

$$f(\mathbf{y}|x) = \prod_{i=1}^N f(y_i^{\text{DC}}|x), \quad (11)$$

where for  $f(y_i^{\text{DC}}|x)$  we recognize the following cases.

Firstly, for the sensitivity area where  $y_i^{\text{DC}} = 0$  and  $k_i = 0$ , with the use of (2) and (7), we have

$$f(y_i^{\text{DC}}) = (1 - e^{-\lambda_x^{\text{DC}} u_{\min}}) \delta(y_i^{\text{DC}}). \quad (12)$$

Secondly, for the linear area, where  $0 < y_i^{\text{DC}} < y_{\text{sat}}$  and  $k_i \in [1, K]$ , with the use of (2) and (8), we have

$$f(y_i^{\text{DC}}) = \lambda_x^{\text{DC}} e^{-\lambda_x^{\text{DC}} k_i \left( \frac{y_i^{\text{DC}}}{\alpha} + u_{\min} \right)}. \quad (13)$$

Furthermore, for the saturation area where  $y_i^{\text{DC}} = y_{\text{sat}}$  with the use of (2) and (9), we consider two cases depending on the number of activated rectifiers

$$f(y_i^{\text{DC}}) = \begin{cases} e^{-\lambda_x^{\text{DC}} k_i u_{\max}} (1 - e^{-\lambda_x^{\text{DC}} u_{\min}}) \delta(y_i^{\text{DC}} - y_{\text{sat}}), & \text{if } k_i \in [1, K], \\ e^{-\lambda_x^{\text{DC}} K u_{\max}} \delta(y_i^{\text{DC}} - y_{\text{sat}}), & \text{if } k_i = K. \end{cases} \quad (14)$$

Therefore, the final decision on the transmitted symbol is based on the following criterion

$$\prod_{i=1}^N f(y_i^{\text{DC}}|0) \underset{\tilde{x}=1}{\overset{\tilde{x}=0}{\geq}} \prod_{i=1}^N f(y_i^{\text{DC}}|1). \quad (15)$$

2) *RF Combiner*: As seen in Fig. 2, the decoding complexity for the RF combiner is lower, since the decoder needs to sample only a small portion of the DC output from only one activated rectifier. On the other hand, the battery is charged with the remaining DC outputs from all the activated rectifiers, i.e.  $(1 - \rho) k y^{\text{RF}}$ . Similarly to the DC combining scheme, by following the same steps, the optimum decision rule is calculated as

$$f(y^{\text{RF}}|0) \underset{\tilde{x}=1}{\overset{\tilde{x}=0}{\geq}} f(y^{\text{RF}}|1), \quad (16)$$

where  $f(y^{\text{RF}}|x)$  can be easily derived from (5), (7), (8) and (9) considering the same methodology as in DC combiner.

### III. SYMBOL ERROR RATE ANALYSIS

In this section, we study the performance of the integrated SWIPT receiver for the ID, in terms of SER.

#### A. DC Combiner

In order to proceed with the analysis, we have to take into consideration that the number of activated rectifiers depends on the received RF power signal. As such, we herein calculate the optimum number of the activated rectifiers for the DC combiner at each receive antenna  $i$ , following the steps from [23].

Firstly, taking into consideration that  $k_i$  is the optimum number of activated rectifiers, the received RF power signal,  $u_i^{\text{DC}}$ , should overpass the sensitivity level,  $u_{\min}$ , for all of them i.e.

$$u_i^{\text{DC}} > k_i u_{\min}. \quad (17)$$

Furthermore, having  $k_i$  activated rectifiers should result in increased DC output, compared to the maximum DC output that can be achieved by  $k_i - 1$  activated rectifiers, i.e. when in the saturation area. Therefore

$$k_i \alpha \left( \frac{u_i^{\text{DC}}}{k_i} - u_{\min} \right) > (k_i - 1) y_{\text{sat}}. \quad (18)$$

On the other hand, in order to avoid activating more than  $k_i$  rectifiers, we should also consider the following condition. The maximum DC output that can be achieved by  $k_i$  activated rectifiers, i.e. when in the saturation area, should be higher compared to the DC output of having  $k_i + 1$  activated rectifiers. As such

$$k_i y_{\text{sat}} \geq (k_i + 1) \alpha \left( \frac{u_i^{\text{DC}}}{k_i + 1} - u_{\min} \right). \quad (19)$$

Consequently, the optimum number of activated rectifiers, is given by

$$k_i = \left\lceil \frac{u_i^{\text{DC}} - u_{\min}}{u_{\max}} \right\rceil. \quad (20)$$

From the above and by taking into consideration the topology in Fig. 1, as well as (7), (8) and (9), we conclude that the received power signal at each antenna  $i$ , activates  $k_i$  rectifiers, whose DC output is either in the sensitivity, the linear or the saturation area.

Considering that the proposed system model consists of  $N$  antennas each one connected to  $K$  rectifiers, we herein make

the following assumption. We accept that the received power signal at  $N_{\text{sen}}$  out of  $N$  antennas, is less than the sensitivity level, thus not activating any rectifiers, i.e.  $k_i = 0$ . On the other hand, at  $N_L$  out of  $N$  antennas the received power signal results in activating  $k_{l_i} \in [1, K]$  rectifiers, with DC output belonging in the linear area. Finally,  $N_{\text{sat1}}$  and  $N_{\text{sat2}}$  out of  $N$  antennas, have  $k_{s_i} \in [1, K - 1]$  and  $k_{s_i} = K$  activated rectifiers, respectively, in the saturation area. Therefore, in the following Theorem we calculate the relative probability, given that  $x$  was transmitted and considering that the DC outputs from the  $N$  antennas are independent to each other.

**Theorem 1.** *The probability regarding the DC outputs from  $N$  receive antennas, given that  $x$  was transmitted, is given as*

$$P_N(x) = e^{-\lambda_x^{\text{DC}} u_{\text{max}}} (K N_{\text{sat2}} + \sum_{l_i=1}^{N_L} k_{l_i} + \sum_{s_i=1}^{N_{\text{sat1}}} k_{s_i}) \times (e^{-\lambda_x^{\text{DC}} (u_{\text{min}} - u_{\text{max}})} - 1) (1 - e^{-\lambda_x^{\text{DC}} u_{\text{min}}})^{(N_{\text{sen}}+1)}, \quad (21)$$

where  $\lambda_x^{\text{DC}}$  is given from (3).

*Proof.* See Appendix A.  $\square$

In order to calculate the total probability of DC outputs from the  $N$  antennas and  $K$  rectifiers, we need also to take into consideration the ordering of the antennas whose DC outputs belong to the sensitivity, linear and saturation areas. As such, we herein introduce the antenna set  $L = (l_1, l_2, \dots, l_{N_L})$ , which indicates the  $N_L$  out of the  $N$  antennas, whose DC outputs are in the linear area with  $k_{l_i} \in [1, K]$  activated rectifiers. Likewise,  $S = (s_1, s_2, \dots, s_{N_{\text{sat1}}})$  indicates the antenna set for the  $N_{\text{sat1}}$  out of the  $N$  antennas that their DC outputs are in the saturation area, with  $k_{s_i} \in [1, K]$  activated rectifiers. Therefore, we herein calculate variable  $C_m$  as follows

$$C_m = \binom{N}{N_{\text{sen}}} \binom{N - N_{\text{sen}}}{N_L} \binom{N - N_{\text{sen}} - N_L}{N_{\text{sat1}}} \times \binom{N - N_{\text{sen}} - N_L - N_{\text{sat1}}}{N_{\text{sat2}}}. \quad (22)$$

Furthermore, we need to consider all possible combinations of  $N_{\text{sen}}$ ,  $N_L$ ,  $N_{\text{sat1}}$  and  $N_{\text{sat2}}$ , given that their sum is equal to  $N$  and  $N_{\text{sen}}, N_L, N_{\text{sat1}}, N_{\text{sat2}} \in [0, N]$ . This is derived by applying the mathematical technique of stars and bars [24] for the pair of  $N$  antennas and  $K$  rectifiers as follows

$$M = \binom{N + 2K}{2K} = \frac{(N + 2K)!}{N!(2K)!}. \quad (23)$$

In order to proceed our analysis with the derivation of the total probability or error, we herein need to consider the ML criterion in (15). Therefore, with the appropriate calculations we have

$$(\lambda_1^{\text{DC}} - \lambda_0^{\text{DC}}) \sum_{l_i=1}^{N_L} u_{l_i}^{\text{DC}} \begin{matrix} \tilde{x}=0 \\ \tilde{x}=1 \end{matrix} + (\lambda_0^{\text{DC}} - \lambda_1^{\text{DC}}) u_{\text{max}} \sum_{k_{s_i}=1}^{N_{\text{sat1}}} k_{s_i} + (\lambda_0^{\text{DC}} - \lambda_1^{\text{DC}}) u_{\text{max}} K N_{\text{sat2}} + \ln \left( \frac{\lambda_1^{\text{DC}}}{\lambda_0^{\text{DC}}} \right)^{N_L} + (N_{\text{sen}} + N_{\text{sat1}}) \ln \left( \frac{1 - e^{-\lambda_1^{\text{DC}} u_{\text{min}}}}{1 - e^{-\lambda_0^{\text{DC}} u_{\text{min}}}} \right). \quad (24)$$

Dividing both parts of the inequality with  $\lambda_1^{\text{DC}} - \lambda_0^{\text{DC}}$ , while taking into consideration that  $\lambda_1^{\text{DC}} < \lambda_0^{\text{DC}}$ , the ML criterion is expressed as

$$z \begin{matrix} \tilde{x}=1 \\ \tilde{x}=0 \end{matrix} \geq t, \quad (25)$$

where  $z = \sum_{l_i=1}^{N_L} u_{l_i}^{\text{DC}}$  and  $t$  equals to the right part of inequality. As such with the use of Theorem 1, (22), (23) and (25) we derive the total probability of error at the following Theorem.

**Theorem 2.** *The total probability of error for DC combining is calculated as*

$$P_e^{\text{DC}} = \frac{1}{2} \sum_{m=1}^M C_m \sum_{x \in (0,1)} \left[ P_{e,z}(x) (1 - e^{-\lambda_x^{\text{DC}} u_{\text{min}}})^{(N_{\text{sen}}+1)} \times e^{-\lambda_x^{\text{DC}} u_{\text{max}}} (K N_{\text{sat2}} + \sum_{s_i=1}^{N_{\text{sat1}}} k_{s_i}) \right], \quad (26)$$

where

- if  $z_{\text{min}} < t \leq z_k$ :

$$P_{e,z}(0) = \frac{e^{-t}}{\Gamma(N_L)} \gamma(N_L, z_k - t) + \frac{e^{-z_{\text{max}}}}{\Gamma(N_L)} \gamma(N_L, z_{\text{max}} - z_k), \quad (27)$$

and

$$P_{e,z}(1) = \frac{e^{-\lambda_1^{\text{DC}} z_{\text{min}}}}{\Gamma(N_L)} \gamma(N_L, \lambda_1^{\text{DC}} (t - z_{\text{min}})), \quad (28)$$

- if  $z_k < t \leq z_{\text{max}}$ :

$$P_{e,z}(0) = \frac{e^{-z_{\text{max}}}}{\Gamma(N_L)} \gamma(N_L, z_{\text{max}} - t), \quad (29)$$

and

$$P_{e,z}(1) = \frac{e^{-\lambda_1^{\text{DC}} z_{\text{min}}}}{\Gamma(N_L)} \gamma(N_L, \lambda_1^{\text{DC}} (z_k - z_{\text{min}})) + \frac{e^{-\lambda_1^{\text{DC}} t}}{\Gamma(N_L)} \gamma(N_L, \lambda_1^{\text{DC}} (t - z_k)). \quad (30)$$

*Proof.* See Appendix B.  $\square$

One can easily note, that the decoding complexity is equal to  $(2K + 1)^N$ , since the output from an antenna  $i$ , might belong either to the sensitivity area or the linear area with  $k_{l_i} \in [1, K]$  activated rectifiers or the saturation area with  $k_{s_i} \in [1, K]$  activated rectifiers, while we have to consider  $N$  such outputs from all the receive antennas. In order to minimize the complexity, at the general context of critical IoT services, we herein examine two simple scenarios regarding the proposed solution.

First of all, we assume that the system model as seen in Fig. 1, consists of  $N$  antennas, each one connected only to one rectifier i.e.  $K = 1$ . Specifically, the decoder samples and optimally combines with the use of ML, the DC outputs from  $N$  rectennas. The DC output from each rectenna might be either in the sensitivity, in the linear or the saturation area. Therefore, by considering all the possible combinations for

the  $N$  rectennas, the decoding complexity is equal to  $3^N$ , which is exponentially increased with the number of antennas. Furthermore, the probability of error is given from Theorem (2), considering that  $K = 1$  and  $N_{sat1} = 0$ .

The second simple scenario that we examine, is the multiple rectifiers scenario. Specifically, we assume that the proposed system model as seen in Fig.1, has only one receive antenna, i.e.  $N = 1$ , which is connected to multiple,  $K$ , rectifiers. As such, the decoder in order to estimate the transmitted symbol  $x$ , considers only one DC output. By taking into account that it might be either in the sensitivity, in the linear or the saturation area, the decoding complexity is equal to  $2K + 1$ , which is linearly increased with the number of rectifiers. The probability of error is given from (2), considering  $N = 1$ .

### B. RF Combiner

We recall that in this scheme, all the received RF signals from the  $N$  antennas are combined and then channeled to the  $K$  rectifiers, in order to be converted to DC signal. As seen in Fig. 2, the received power signal  $u^{\text{RF}}$ , is then equally split to  $K$  rectifiers. The optimal number of activated rectifiers is denoted as  $k$  and is calculated following the exact same methodology as in RF combining scheme. Similarly to the DC combining scenario, the DC output might be either in the sensitivity, the linear or the saturation area.

In order to proceed our analysis with the calculation of the probability of error in terms of SER, we have to consider the ML criterion from (16). With the appropriate substitutions and calculations, the ML decision rule follows

$$u^{\text{RF}} \underset{\tilde{x}=0}{\overset{\tilde{x}=1}{\geq}} \frac{PN+1}{PN} \ln(PN+1), \quad (31)$$

where we set the right part of the inequality equal to  $z_{\text{RF}}$ . As such, the relative probability of error, follows in the next Theorem.

**Theorem 3.** *The total probability of error for the proposed system model of RF combining is*

$$\begin{aligned} P_e^{\text{RF}} = & \frac{1}{2} \left[ 1 - e^{-\lambda_1^{\text{RF}} u_{\min}} + e^{-\lambda_0^{\text{RF}} K u_{\max}} \right. \\ & + \sum_{k=1}^{K-1} e^{-\lambda_{\tilde{x}'}^{\text{RF}} k u_{\max}} (1 - e^{-\lambda_{\tilde{x}'}^{\text{RF}} u_{\min}}) \\ & + \sum_{k=1}^K e^{-\lambda_0^{\text{RF}} (u_{\min} + (k-1)u_{\max})} - K e^{-\lambda_0^{\text{RF}} z_{\text{RF}}} \\ & \left. - \sum_{k=1}^{K-1} e^{-\lambda_1^{\text{RF}} k u_{\max}} + (K-1)e^{-\lambda_1^{\text{RF}} z_{\text{RF}}} \right], \quad (32) \end{aligned}$$

where  $\tilde{x}'$  denotes the symbol that was not estimated.

*Proof.* See Appendix C.  $\square$

Herein, one can easily notice that the decoding complexity is equal to  $2K + 1$ , since we take into consideration the DC output from one rectifiers, where its output might be either in the sensitivity, the linear or saturation area with  $k \in [1, K]$  activated rectifiers. At this point we introduce the simplest solution for the proposed RF combining scheme. In this

scenario, we assume that the system model as seen in Fig.2, consists of  $N$  antennas, where after combining the received signals in the RF domain, the power signal is channeled to  $K = 1$  rectifier. Herein, the decoding complexity is equal to three, which is independent from the number of antennas  $N$ . Clearly, the decoding complexity in this scenario is less than the corresponding scenario in DC combining, where the two proposed system models consist of the same number of antennas and rectifiers i.e.  $N$  and  $K = 1$ . The probability of error is given from Theorem 3, considering  $K = 1$ .

The second simplest scenario that we examine is by assuming that the proposed system model as seen in Fig.2, has only one receive antenna, i.e.  $N = 1$  and is connected to multiple,  $K$ , rectifiers. One can easily notice, that this scenario is the same with the corresponding scenario of the DC combining scheme. Therefore, this scenario is common for the DC and RF combining schemes.

## IV. AVERAGE ENERGY HARVESTING

In this section, we present the average EH, denoted by  $Q$  and measured in Joule, for both schemes. The average EH from an antenna  $i$ , given that  $x$  is transmitted, is calculated by the sum of expected values of the DC outputs, for all the  $K$  activated rectifiers. Therefore

$$Q = \sum_{x \in (0,1)} \mathbb{P}(x) \mathbb{E}[y_i(u_i)] = \frac{1}{2} \sum_{x \in (0,1)} \int_{u_{\min}}^{\infty} y_i(u_i) f(u_i) du_i, \quad (33)$$

where we note that the power of AWGN is too weak to be harvested, as such it is omitted. As such in the following two Propositions we calculate the average EH for the DC and RF combining scheme, respectively.

**Proposition 1.** *For the DC combining scheme the average EH is calculated as*

$$\begin{aligned} Q^{\text{DC}} = & \frac{N}{2} \sum_{x \in (0,1)} \left[ K y_{\text{sat}} e^{-\lambda_x^{\text{DC}} K u_{\max}} \right. \\ & + y_{\text{sat}} (1 - e^{-\lambda_x^{\text{DC}} u_{\min}}) \sum_{s_i=1}^{K-1} k_{s_i} e^{-\lambda_x^{\text{DC}} k_{s_i} u_{\max}} \\ & + \frac{1}{\lambda_x^{\text{DC}}} \sum_{l_i=1}^K e^{-\lambda_x^{\text{DC}} k_{l_i} u_{\max}} \left( -\alpha - \lambda_x^{\text{DC}} k_{l_i} y_{\text{sat}} \right. \\ & \left. \left. - e^{\lambda_x^{\text{DC}} (u_{\max} - u_{\min})} (\lambda_x^{\text{DC}} y_{\text{sat}} (1 - k_{l_i}) - \alpha) \right) \right], \quad (34) \end{aligned}$$

where we recall that  $y_{\text{sat}} = \alpha(u_{\max} - u_{\min})$ .

*Proof.* For the DC combining scheme and the calculation of the average EH, we should consider the DC outputs from  $N$  antennas. Therefore, by substituting in (33) the values of  $y_i^{\text{DC}}$  from (7), (8), (9) and  $f(y_i^{\text{DC}})$  from (12), (13), (14) respectively, (34) is proven with the appropriate calculations.  $\square$

**Proposition 2.** *For the RF combining scheme the average EH is calculated as*

$$Q^{\text{RF}} = \frac{1}{2} \sum_{x \in (0,1)} \left[ K y_{\text{sat}} e^{-\lambda_x^{\text{RF}} K u_{\max}} \right]$$

$$\begin{aligned}
& + y_{sat} \left( 1 - e^{-\lambda_x^{\text{RF}} u_{\min}} \right) \sum_{s_i=1}^{K-1} k_i e^{-\lambda_x^{\text{RF}} k_{s_i} u_{\max}} \\
& + \frac{1}{\lambda_x^{\text{RF}}} \sum_{l_i=1}^K e^{-\lambda_x^{\text{RF}} k_{l_i} u_{\max}} \left( -\alpha - \lambda_x^{\text{RF}} k_{l_i} y_{sat} \right. \\
& \left. - e^{\lambda_x^{\text{RF}} (u_{\max} - u_{\min})} (\lambda_x^{\text{RF}} y_{sat} (1 - k_{l_i}) - \alpha) \right) \Bigg]. \quad (35)
\end{aligned}$$

The above proposition is derived similarly to Proposition 1 and so we omit the proof. Furthermore, the average EH for the proposed simple scenarios is given from (34) and (35), considering that  $K = 1$  and  $N_{\text{sat}1} = 0$  or  $N = 1$ , accordingly.

## V. ASYMPTOTIC ANALYSIS

In this paragraph, we examine the behavior of our system models asymptotically, in high average transmitted power regime, considering an infinite number of receive antennas  $N$  and a large number of rectifiers  $K$ .

### A. DC combining

When  $P \rightarrow \infty$ , a lower bound, in terms of SER, is calculated as expressed in the following Corollary.

**Corollary 1.** *A lower bound, in terms of SER, for the DC combining scheme is derived as follows*

$$\lim_{P \rightarrow \infty} P_e^{\text{DC}} = \frac{1}{2} e^{-N K u_{\max}}. \quad (36)$$

*Proof.* For really high values of  $P$ , all the available  $K$  rectifiers at an antenna  $i$  will be activated and reached the saturation area, with probability equal to  $\mathbb{P}(K u_{\max} \leq u_i^{\text{DC}})$ , as given from (46) in Appendix A. This applies for the DC outputs from all  $N$  receive antennas. Therefore,  $N_{\text{sat}2} = N$ , while  $N_{\text{sen}} = N_L = N_{\text{sat}1} = 0$  and Theorem 1 results in

$$P_N(x) = (\mathbb{P}(K u_{\max} \leq u_i^{\text{DC}}))^N = e^{-\lambda_x^{\text{DC}} K u_{\max} N}. \quad (37)$$

Considering the ML condition from (24), with the appropriate substitutions and calculations we see that the estimated transmitted symbol, will always be equal to  $\tilde{x} = 1$ . As such, the bound for the relative probability of error is

$$\lim_{P \rightarrow \infty} P_e^{\text{DC}} = \frac{1}{2} e^{-\lambda_0^{\text{DC}} N K u_{\max}}. \quad (38)$$

Considering that  $\lambda_0^{\text{DC}} = 1$ , the result in (36) follows.  $\square$

Regarding the EH, for high values of  $P$ , we derive an upper bound as expressed in the following Proposition.

**Proposition 3.** *An upper bound regarding the EH and the DC combining scheme is derived as follows*

$$\begin{aligned}
\lim_{P \rightarrow \infty} Q^{\text{DC}} &= \frac{N}{2} \left[ K y_{sat} (1 + e^{-K u_{\max}}) \right. \\
&+ y_{sat} (1 - e^{-u_{\min}}) \sum_{s_i=1}^{K-1} k_{s_i} e^{-k_{s_i} u_{\max}} \\
&\left. - \sum_{l_i=1}^K e^{-k_{l_i} u_{\max}} \left( \alpha + k_{l_i} y_{sat} \right. \right.
\end{aligned}$$

$$\left. \left. + e^{(u_{\max} - u_{\min})} (y_{sat} (1 - k_{l_i}) - \alpha) \right) \right]. \quad (39)$$

*Proof.* For  $P \rightarrow \infty$ , the rate parameter given that  $x = 1$ , results in  $\lambda_1^{\text{DC}} = 0$ . By taking into consideration the property that for small values of  $x$  applies that  $\exp(-x) \approx 1 - x$ , then (39) is derived directly from (34).  $\square$

The relative bounds for the simple scenarios of  $N = 1$  and  $K = 1$ , are obtained from (36) and from (39), by considering  $N = 1$  and  $K = 1$ , respectively.

Furthermore, we herein note, that when the number of receive antennas  $N$ , tends asymptotically to infinity, the performance of ID and EH, will asymptotically tend to zero and infinity, respectively. This can be easily derived from Theorem 2 and Proposition 1, considering that for  $N \rightarrow \infty$ , then also  $N_{\text{sen}}$ ,  $N_L$ ,  $N_{\text{sat}1}$  and  $N_{\text{sat}2}$  tend asymptotically to infinity. Finally, considering a large number of  $K$  rectifiers at each receive antenna, will result in a DC output that will never reach the saturation area. As such, the ID could be calculated from Theorem 2, considering  $N_{\text{sat}2} = 0$ . Similarly, the EH could be calculated from Proposition 1, by omitting the term of  $K y_{sat} e^{-\lambda_x^{\text{DC}} K u_{\max}}$ .

### B. RF combining

For high values of  $P$ , as in the DC combining scheme, a lower bound in terms of SER is calculated, while for the EH an upper bound is derived.

**Remark 1.** *For  $P \rightarrow \infty$ , the total probability of error, in terms of SER, for the RF combining scheme converges to*

$$\lim_{P \rightarrow \infty} P_e^{\text{RF}} = \frac{1}{2} e^{-K u_{\max}}. \quad (40)$$

*Proof.* As in the DC combining scheme, due to the high average received power, all the available  $K$  rectifiers will be activated in the saturation area. Therefore, following the same steps as in Corollary 1, (40) results directly from (36) by substituting  $N = 1$ .  $\square$

One can easily note, that the performance of the RF combining scheme in terms of SER, increases as the number of rectifiers  $K$  increase and is independent from the number of receive antennas  $N$ .

**Remark 2.** *For  $P \rightarrow \infty$ , the average EH for the RF combining scheme converges to*

$$\begin{aligned}
Q_{\text{bnd}}^{\text{RF}} &= \frac{1}{2} \left[ K y_{sat} (1 + e^{-K u_{\max}}) \right. \\
&+ y_{sat} (1 - e^{-u_{\min}}) \sum_{k=1}^{K-1} k e^{-k u_{\max}} \\
&- \sum_{k=1}^K e^{-k u_{\max}} \left( \alpha + k y_{sat} \right. \\
&\left. \left. + e^{(u_{\max} - u_{\min})} (y_{sat} (1 - k) - \alpha) \right) \right], \quad (41)
\end{aligned}$$



TABLE II  
SIMULATION PARAMETERS

Description	Notation & Value	Description	Notation & Value
Sensitivity power level	$u_{\min} = 0.1$	Saturation power level	$u_{\max} = 2$
Conversion efficiency from RF to DC	$\alpha = 0.7$ [40]	Monte-Carlo	$10^6$ iterations
Number of receive antennas	$N = 2$	Number of rectifiers	$K = 2$

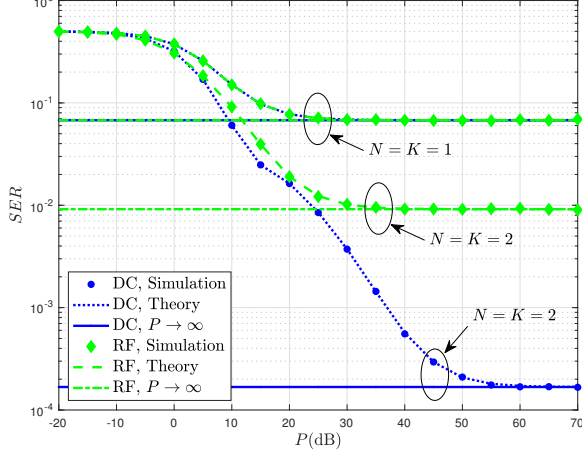


Fig. 3. SER of the integrated SWIPT receiver, for  $N = K = 2$  and  $N = 1, K = 1$ , for DC and RF combining.

where result follows from (35), considering that  $\lambda_1^{\text{DC}} = 0$  and following the same steps as in Proposition 3.

From (39) and (41), we can easily notice that

$$Q_{\text{bnd}}^{\text{RF}} = \frac{Q_{\text{bnd}}^{\text{DC}}}{N}. \quad (42)$$

The relative bounds for the scenarios of  $K = 1$  and  $N = 1$ , are obtained from (40) and from (41), by considering  $K = 1$  and  $N = 1$ , respectively.

Furthermore, we herein note that considering an infinite number of receive antennas results in the same asymptotic analysis as if  $P \rightarrow \infty$ , both for ID and EH. Finally, for a large number of rectifiers,  $K$ , the DC output will never reach the saturation area. Therefore, from Theorem 3 we could calculate the ID, by omitting the term of  $\mathbb{P}(u^{\text{RF}} > Ku_{\max}|x=0) = e^{-\lambda_0^{\text{RF}} Ku_{\max}}$ . Following the same approach, the EH could be calculated from Proposition 2, by omitting the term of  $Ky_{\text{sat}}e^{-\lambda_x^{\text{RF}} Ku_{\max}}$ .

## VI. NUMERICAL RESULTS

In this section, we provide numerical results and illustrate the performance of our system model. Monte-Carlo simulations are carried out and all the outcomes presented are calculated for  $10^6$  iterations. The main simulation parameters used in the paper, are summarized in Table II.

Fig. 3, presents the performance of the integrated SWIPT receiver in terms of SER, considering  $N = K = 2$ , for DC and RF combining. Furthermore, we illustrate their performance for  $N = K = 1$ , as the solution with the simplest complexity. Finally, we present the lower bound as calculated from the

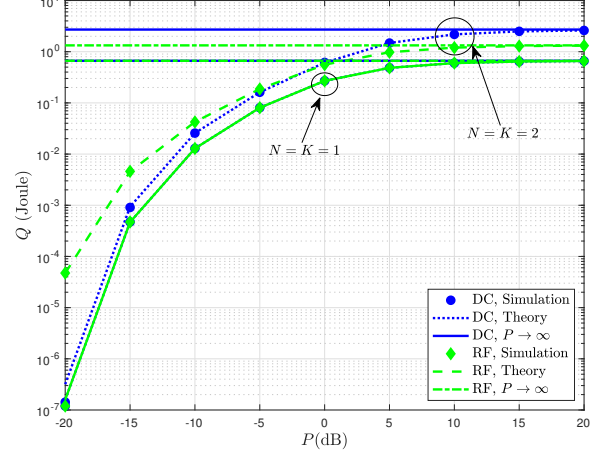


Fig. 4. EH of the integrated SWIPT receiver, for  $N = K = 2$  and  $N = 1, K = 1$ , for DC and RF combining.

asymptotic analysis, considering  $P \rightarrow \infty$ . Clearly, enhanced decoding performance is succeeded by increasing  $N$  and  $K$ . Specifically, when referring to DC combining scheme this results in more samples per symbol, but still the complexity of sampling is not so high with the current state-of-the-art of analog digital converters (ADCs) [41]. Furthermore, DC combining has an enhanced performance compared to RF combining, for the same number of receive antennas,  $N$ , and rectifiers,  $K$ .

In Fig. 4, we illustrate the performance of the system model in terms of EH, for  $N = K = 2$ , as well as for  $N = K = 1$ . We notice that the proposed solution for DC combining increases the EH and offers enhanced results compared to RF combining, when referring to high power regime, while this inverses at low power. Furthermore, we see that the EH in the DC combining is  $N = 2$  times higher than the EH in the RF combining, for the same number of rectifiers  $K = 2$ , as asymptotically  $P \rightarrow \infty$ .

In Fig. 5 and 6, we present the performance of the simple case scenarios, in terms of SER and EH. From Fig. 5, one can easily note that the best performance in terms of SER, when  $K = 1$ , is for the RF scenario with the least decoding complexity, specifically when referring to the low range of transmitted power  $P$ , while this is reverted as  $P$  increases. On the other hand, for the case of  $N = 1$ , both RF and DC combining schemes have exactly the same behavior, since the two proposed topologies are the same. Furthermore, for the DC combining scheme we see that the increase in the number of antennas  $N = 2, K = 1$ , compared to the increase in the number of rectifiers i.e  $N = 1, K = 2$ , results in

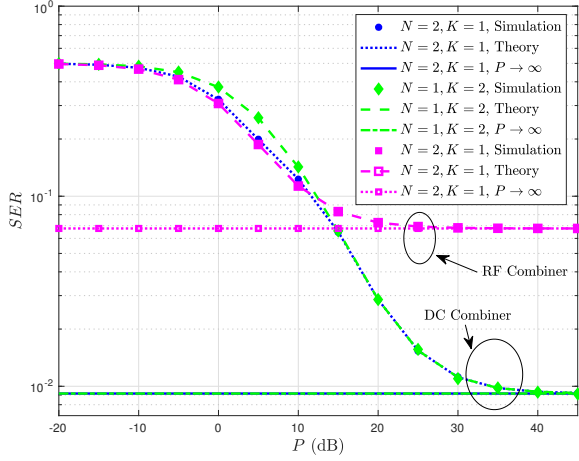


Fig. 5. SER of the integrated SWIPT receiver, for the simple cases of  $N = 1, K = 2$  and  $N = 2, K = 1$ .

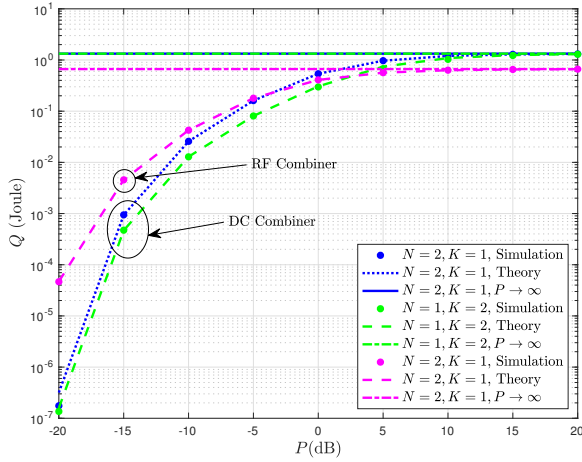


Fig. 6. EH of the integrated SWIPT receiver, for the simple cases of  $N = 1, K = 2$  and  $N = 2, K = 1$ .

better performance in low power regime, while asymptotically perform the same.

Fig. 6 highlights the enhanced performance of the DC combining scheme in terms of EH, when we increase the number of antennas  $N = 2, K = 1$  compared to the increase in the number of rectifiers  $N = 1, K = 2$ , specifically referring to the low power regime. We notice that in the scenario of  $N = 2, K = 1$ , the EH increases linearly with the number of rectennas, while this is not the case for the case of  $N = 1, K = 2$ . Furthermore, we observe that the case of  $N = 2, K = 1$  in the RF combining scheme has the better performance in low power regime and it is upper bounded by the performance of DC combining, considering  $N = K = 1$ .

In Fig. 7 we illustrate the performance in terms of SER for the DC and RF combining scheme, as per transmitted average power  $P$  and power levels  $u_{\min}$  and  $u_{\max}$ . It is interesting that for the DC combining scheme, the SER deteriorates with the increase of sensitivity power level when in low power

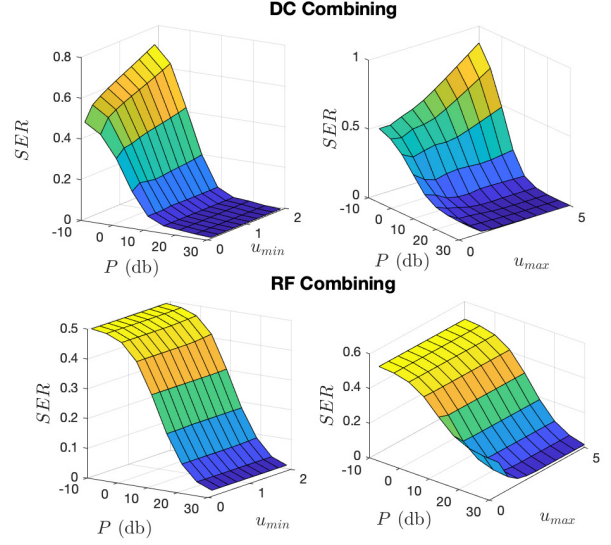


Fig. 7. Performance DC and RF combining for  $N = K = 2$ , in terms of  $SER, P, u_{\min}$  and  $u_{\max}$ .

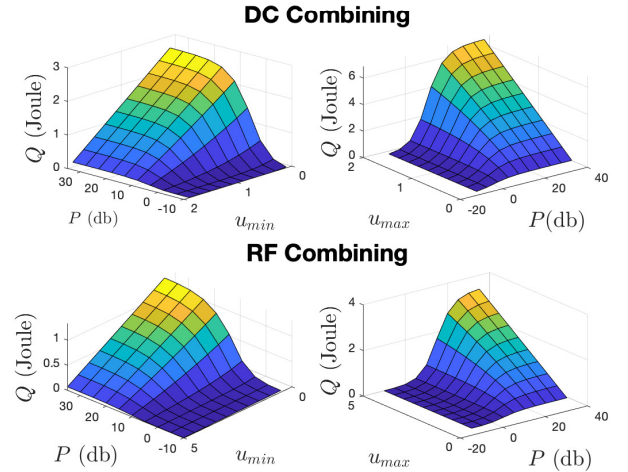


Fig. 8. Performance DC and RF combining for  $N = K = 2$ , in terms of  $Q, P, u_{\min}$  and  $u_{\max}$ .

regime. On the other hand, as  $P$  increases and we reach the lower bound of SER, the variation of  $u_{\min}$  does not affect the performance. Regarding the variations in the  $u_{\max}$ , we notice that there is a small range that maximizes the SER, while after that any increase deteriorates the performance, till it reaches the saturation area. For the RF combining scheme, we observe that the variations in  $u_{\min}$  and  $u_{\max}$  hardly affect the performance of SER. This is due to the fact, that the received RF power signal is summed from the  $N$  antennas and then channeled to the rectifiers. Finally, compared to the DC combining scheme and for the same power levels, specifically referring to the low regime, it is noticed that for high values of sensitivity and saturation levels the RF combining scheme surpasses the DC combining scheme.

In Fig. 8 we present the performance of DC and RF combining scheme, in terms of EH and how this is affected

by variation of  $P$ ,  $u_{\min}$  and  $u_{\max}$ . We can clearly notice that as the transmitted power,  $P$ , and the saturation power level,  $u_{\max}$ , increase, the EH for the DC combining scheme increases as well. On the contrary, for the same levels of average transmitted power  $P$ , the increase in the sensitivity power level,  $u_{\min}$ , affects negatively the EH. Finally, the same behavior is observed for the RF combining scheme, though the EH is less compared to the DC combining scheme, as already noted in Fig. 4.

## VII. CONCLUSION

In this work, we study a non-coherent detection scheme for integrated SWIPT receivers. We consider two SIMO topologies with  $N$  receive antennas and  $K$  rectifiers, examining a DC and RF combining scheme, respectively. The proposed system models, by using a ML-based soft decoding, exploit simultaneously the rectified DC power signal, jointly enhancing the performance of ID and EH. In addition, with the use of a piecewise linear EH model, we manage to capture the sensitivity and saturation behavior of the rectifiers. In particular it is shown, that for the same number of receive antennas,  $N$ , and rectifiers,  $K$ , the DC combining scheme surpasses the RF combining scheme, in terms of SER, while this results in increased decoding complexity compared to the RF scheme. Regarding the average EH, DC combining scheme is superior at high power regime while this differentiates at low values of  $P$ . Finally, we conduct an asymptotic analysis, providing lower and upper bounds, for the ID and EH, respectively. Simulation and theoretical results are consistent, corroborating our study.

### APPENDIX A PROOF OF THEOREM 1

From (2) and taking into consideration the cumulative density function, we herein calculate the probabilities regarding the DC output from an antenna  $i$ . Specifically, the probability of DC output being in the sensitivity area is calculated by taking into consideration that the received RF power signal is less than the sensitivity level,  $u_{\min}$ , therefore the rectifier is not activated resulting in  $k_i = 0$ . As such

$$\mathbb{P}(u_i^{\text{DC}} < u_{\min}) = F_{u_i^{\text{DC}}}(u_{\min}) = 1 - e^{-\lambda_x^{\text{DC}} u_{\min}}. \quad (43)$$

Furthermore, the probability of the DC output belonging to the linear area, is interwoven with the probability that the received RF power signal is higher than the sensitivity level,  $u_{\min}$  and less than the saturation level,  $u_{\max}$ . As such, based on the level of the received power signal  $k_{l_i} \in [1, K]$  rectifiers are activated. Therefore

$$\begin{aligned} \mathbb{P}(u_{\min} + (k_{l_i} - 1)u_{\max} \leq u_i^{\text{DC}} < k_{l_i}u_{\max}) \\ = F_{u_i^{\text{DC}}}(u_{\max}) - F_{u_i^{\text{DC}}}(u_{\min}) \\ = e^{-\lambda_x^{\text{DC}} k_{l_i} u_{\max}} (e^{-\lambda_x^{\text{DC}} (u_{\min} - u_{\max})} - 1). \end{aligned} \quad (44)$$

In addition, the probability that the received RF power signal is at such levels that results in activating  $k_{s_i} \in [1, K - 1]$  rectifiers in the saturation area, is calculated as

$$\mathbb{P}(k_{s_i}u_{\max} \leq u_i^{\text{DC}} < k_{s_i}u_{\max} + u_{\min})$$

$$\begin{aligned} &= F_{u_i^{\text{DC}}}(u_{\max} + u_{\min}) - F_{u_i^{\text{DC}}}(u_{\max}) \\ &= e^{-\lambda_x^{\text{DC}} k_{s_i} u_{\max}} (1 - e^{-\lambda_x^{\text{DC}} u_{\min}}). \end{aligned} \quad (45)$$

Finally, the probability of activating all the rectifiers in the saturation area follows

$$\mathbb{P}(Ku_{\max} \leq u_i^{\text{DC}}) = \bar{F}_{u_i^{\text{DC}}}(Ku_{\max}) = e^{-\lambda_x^{\text{DC}} Ku_{\max}}. \quad (46)$$

Therefore the probability regarding the DC outputs from  $N$  receive antennas, given that  $x$  was transmitted and assuming that  $N_{\text{sen}}$  out of  $N$  antennas are in the sensitivity area,  $N_L$  out of  $N$  antennas in the linear area,  $N_{\text{sat1}}$  and  $N_{\text{sat2}}$  out of  $N$  antennas in the saturation area, follows

$$\begin{aligned} P_N(x) &= (\mathbb{P}(u_i^{\text{DC}} < u_{\min}))^{N_{\text{sen}}} (\mathbb{P}(Ku_{\max} \leq u_i^{\text{DC}}))^{N_{\text{sat2}}} \\ &\times \prod_{l_i=1}^{N_L} \mathbb{P}(u_{\min} + (k_{l_i} - 1)u_{\max} \leq u_i^{\text{DC}} < k_{l_i}u_{\max}) \\ &\times \prod_{s_i=1}^{N_{\text{sat1}}} \mathbb{P}(k_{s_i}u_{\max} \leq u_i^{\text{DC}} < k_{s_i}u_{\max} + u_{\min}). \end{aligned} \quad (47)$$

With the use of probabilities from (43), (44), (45), (46) and the appropriate calculations, we derive (21) in Theorem 1.

### APPENDIX B PROOF OF THEOREM 2

From (24) and (25), it is clearly noticed that  $z$  is the sum of  $N_L$  independent and identically distributed random variables. Furthermore, these variables are exponentially distributed with the same rate parameter, i.e.  $\lambda_x^{\text{DC}}$ . As such, by considering [42, Ch.1.8.7], we conclude that  $z$  follows the Erlang distribution, which results in

$$\begin{aligned} \mathbb{P}(Z < z_k) &= \int_{z_{\min}}^{z_k} \frac{(\lambda_x^{\text{DC}})^{N_L} (z - z_{\min})^{N_L-1}}{\Gamma(N_L)} e^{-\lambda_x^{\text{DC}} z} dz \\ &\stackrel{(a)}{=} \frac{e^{-\lambda_x^{\text{DC}} z_{\min}}}{\Gamma(N_L)} \gamma(N_L, \lambda_x^{\text{DC}} (z_k - z_{\min})), \end{aligned} \quad (48)$$

and

$$\begin{aligned} \mathbb{P}(Z > z_k) &= \int_{z_k}^{z_{\max}} \frac{(\lambda_x^{\text{DC}})^{N_L} (z_{\max} - z)^{N_L-1}}{\Gamma(N_L)} e^{-\lambda_x^{\text{DC}} z} dz \\ &\stackrel{(b)}{=} \frac{e^{-\lambda_x^{\text{DC}} z_{\max}}}{\Gamma(N_L)} \gamma(N_L, \lambda_x^{\text{DC}} (z_{\max} - z_k)), \end{aligned} \quad (49)$$

where (a) and (b) follow from integrating by substituting variables  $z - z_{\min}$  and  $z_{\max} - z$  with variable  $w$ , respectively. Furthermore

$$z_{\min} = N_L u_{\min} + \sum_{l_i=1}^{N_L} (k_{l_i} - 1)u_{\max}, \quad (50)$$

$$z_{\max} = \sum_{l_i=1}^{N_L} k_{l_i} u_{\max}, \quad (51)$$

$$z_k = k_{l_1} u_{\max} + \sum_{l_i=2}^{N_L} (u_{\min} + (k_{l_i} - 1)u_{\max}), \quad (52)$$

while  $z_k$  follows from the individual limits of each independent random variable  $u_{l_i}$  in the sum of  $z$ . Taking into consideration that  $1 \leq N_L \leq N$  and  $k_{l_i} \in [1, K]$  we define

$$u_{\min} \leq z_{\min} \leq Nu_{\min} + N(K-1)u_{\max}, \quad (53)$$

$$u_{\min} + u_{\max} \leq z_{\max} \leq NKu_{\max}, \quad (54)$$

$$u_{\min} + u_{\max} \leq z_k \leq NKu_{\max} - (N-1)(u_{\max} - u_{\min}). \quad (55)$$

Consequently, depending on the values of  $t$  from (25), we proceed accordingly with the calculation of probability of error for  $z$ , i.e.  $P_{e,z}(x)$ . Specifically, we recognize the following two cases.

- if  $z_{\min} < t \leq z_k$ : The probability of error is

$$P_{e,z}(0) \stackrel{(c)}{=} \mathbb{P}(t < z \leq z_k | x = 0) \\ + \mathbb{P}(z_k < z \leq z_{\max} | x = 0), \quad (56)$$

and

$$P_{e,z}(1) \stackrel{(c)}{=} \mathbb{P}(z_{\min} < z \leq t | x = 1), \quad (57)$$

where (c) follows from (48) and (d) from (49).

- if  $z_k < t \leq z_{\max}$ : The probability of error is

$$P_{e,z}(0) \stackrel{(e)}{=} \mathbb{P}(t < z \leq z_{\max} | x = 0), \quad (58)$$

and

$$P_{e,z}(1) \stackrel{(f)}{=} \mathbb{P}(z_{\min} < z \leq z_k | x = 1) \\ + \mathbb{P}(z_k < z \leq t | x = 1), \quad (59)$$

where (e) follows from (49) and (f) from (48).

Therefore, by taking into consideration the transmitted symbol  $x$ , the ML criterion and all possible combinations and ordering of  $N_{\text{sen}}, N_L, N_{\text{sat}1}, N_{\text{sat}2}$ , the total probability of error is calculated as follows

$$P_e^{\text{DC}} = \mathbb{P}(x = 0) \sum_{m=1}^M C_m P_{e,z}(0) \\ \times \prod_{s_i=1}^{N_{\text{sat}1}} \mathbb{P}(k_{s_i} u_{\max} \leq u_i^{\text{DC}} < k_{s_i} u_{\max} + u_{\min}) \\ \times (\mathbb{P}(u_i^{\text{DC}} < u_{\min}))^{N_{\text{sen}}} (\mathbb{P}(Ku_{\max} \leq u_i^{\text{DC}}))^{N_{\text{sat}2}} \\ + \mathbb{P}(x = 1) \sum_{m=1}^M C_m P_{e,z}(1) \\ \times \prod_{s_i=1}^{N_{\text{sat}1}} \mathbb{P}(k_{s_i} u_{\max} \leq u_i^{\text{DC}} < k_{s_i} u_{\max} + u_{\min}) \\ \times (\mathbb{P}(u_i^{\text{DC}} < u_{\min}))^{N_{\text{sen}}} (\mathbb{P}(Ku_{\max} \leq u_i^{\text{DC}}))^{N_{\text{sat}2}}.$$

Then, the final expression in Theorem 2 can be easily obtained, by taking into consideration  $P_{e,z}(x)$  from (56), (57), (58) and (59), with the appropriate substitutions from (43), (45), (46) and (48) or (49).

## APPENDIX C PROOF OF THEOREM 3

By taking into consideration (31), the probability of error is given by

$$P_e^{\text{RF}} = \mathbb{P}(u^{\text{RF}} > z_{\text{RF}} | x = 0) + \mathbb{P}(u^{\text{RF}} < z_{\text{RF}} | x = 1) \\ \stackrel{(g)}{=} \mathbb{P}(u^{\text{RF}} < u_{\min} | x = 1) \\ + \sum_{k=1}^K \mathbb{P}((k-1)u_{\max} + u_{\min} \leq u^{\text{RF}} < z_{\text{RF}} | x = 1) \\ + \sum_{k=1}^K \mathbb{P}(z_{\text{RF}} \leq u_{\text{RF}} < ku_{\max} | x = 0) \\ + \sum_{k=1}^{K-1} \mathbb{P}(ku_{\max} \leq u^{\text{RF}} < ku_{\max} + u_{\min} | x = \hat{x}') \\ + \mathbb{P}(u^{\text{RF}} > Ku_{\max} | x = 0), \quad (60)$$

where (g) follows considering that the DC output signal is in the sensitivity area, (h) in the linear, and (i) in the saturation area. With the use of (43), (44), (45), (46) and the appropriate calculations, Theorem 3 is derived.

## REFERENCES

- [1] E. Goudeli, C. Psomas, I. Krikidis, H. Kiani, D. Chatzichristodoulou, and S. Nikolaou, "Detection schemes for integrated SWIPT receivers with non-linear energy harvesting," *IEEE Veh. Tech. Conf.*, Helsinki, Finland, 2022.
- [2] K. W. Choi, L. Ginting, A. A. Aziz, D. Setiawan, J. H. Park, S. I. Hwang, D. S. Kang, M.Y. Chung, and D. I. Kim, "Toward realization of long-range wireless-powered sensor networks," *IEEE Wireless Commun.*, vol. 26, pp. 184–192, Aug. 2019.
- [3] K. W. Choi, S. I. Hwang, A. A. Aziz, H. H. Jang, J. S. Kim, D. S. Kang, and D. I. Kim, "Simultaneous wireless information and power transfer for internet of things: Novel receiver design and experimental validation," *IEEE Intern. Thin. J.*, vol. 7, pp. 2996–3012, Apr. 2020.
- [4] X. Gu, S. Hemour, and K. Wu, "Far-field wireless power harvesting: Nonlinear modeling, rectenna design, and emerging applications," *Proc. of the IEEE*, vol. 110, pp. 56–73, Jan. 2022.
- [5] M. Rajabi, N. Pan, S. Claessens, S. Pollin, and D. Schreurs, "Modulation techniques for simultaneous wireless information and power transfer with an integrated rectifier-receiver," *IEEE Trans. Micr. Theor. Techn.*, vol. 66, pp. 2373–2385, May 2018.
- [6] J. Kim and B. Clerckx, "Wireless information and power transfer for IoT: Pulse position modulation, integrated receiver, and experimental validation," *arXiv:2104.08404*, 2021.
- [7] I. Krikidis and C. Psomas, "Tone-index multisine modulation for SWIPT," *IEEE Signal Proces. Lett.*, vol. 26, pp. 1252–1256, 2019.
- [8] S. Claessens, N. Pan, M. Rajabi, D. Schreurs, and S. Pollin, "Enhanced biased ask modulation performance for SWIPT with awgn channel and dual-purpose hardware," *IEEE Trans. Micr. Theor. and Techn.*, vol. 66, pp. 3478–3486, July 2018.
- [9] T. D. P. Perera, D. N. K. Jayakody, S. K. Sharma, S. Chatzinotas, and J. Li, "Simultaneous wireless information and power transfer (SWIPT): Recent advances and future challenges," *IEEE Comm. Surv. & Tutor.*, vol. 20, pp. 264–302, Dec. 2017.
- [10] X. Zhou, R. Zhang, and C. K. Ho, "Wireless information and power transfer: Architecture design and rate-energy tradeoff," *IEEE Trans. Commun.*, vol. 61, pp. 4757–4767, Nov. 2013.
- [11] Y. Wu, Q. Yang, and K. S. Kwak, "Energy efficiency maximization for energy harvesting millimeter wave systems at high SNR," *IEEE Wirel. Commun. Lett.*, vol. 6, pp. 698–701, 2017.
- [12] S. Shen, Y. Zhang, C. Chiu, and R. Murch, "A triple-band high-gain multibeam ambient RF energy harvesting system utilizing hybrid combining," *IEEE Trans. Ind. Electron.*, vol. 67, pp. 9215–9226, 2020.
- [13] L. Zheng, and D.N.C. Tse, "Diversity and multiplexing: a fundamental tradeoff in multiple-antenna channels," *IEEE Trans. Inf. Theory*, vol. 49, pp. 1073–1096, 2003.

- [14] I. E. Telatar, "Capacity of multi-antenna gaussian channels," *Europ. Trans. Telecommu.*, vol. 10, pp. 585–595, 1999.
- [15] G. Foschini, G. Golden, R. Valenzuela, and P. Wolniansky, "Simplified processing for high spectral efficiency wireless communication employing multi-element arrays," *IEEE J. Select. Areas Commun.*, vol. 17, pp. 1841–1852, 1999.
- [16] N. Garg, J. Zhang, and T. Ratnarajahe, "Rate-energy balanced precoding design for SWIPT based two-way relay systems," *IEEE J. Select. Top. in Sign. Proc.*, vol. 15, pp. 1228–1241, 2021.
- [17] H. Lee, K. J. Lee, H. Kim, and I. Lee, "Multi-antenna SWIPT systems with joint time switching," *IEEE Int. Conf. Comm.*, Kansas, USA, 2018.
- [18] S. Wang, L. Ma, and W. Wu, "Joint TS beamforming and hybrid TS-PS receiving design for SWIPT systems," *IEEE Access*, vol. 9, pp. 50686–50699, 2021.
- [19] C. Psomas, and I. Krikidis, "A wireless powered feedback protocol for opportunistic beamforming using rectenna arrays," *IEEE Trans. Gr. Comm. and Netw.*, vol. 2, pp. 100–113, 2018.
- [20] S. Shen, and Bruno Clerckx, "Beamforming optimization for MIMO wireless power transfer with nonlinear energy harvesting: RF combining versus DC combining," *IEEE Trans. Wirel. Commun.*, vol. 20, pp. 199–213, 2021.
- [21] U. Olgun, et al., "Investigation of rectenna array configurations for enhanced RF power harvesting," *IEEE Antennas Wireless Propag. Lett.*, vol. 10, pp. 262–265, 2011.
- [22] D.J. Lee, et al., "Hybrid power combining rectenna array for wide incident angle coverage in RF energy transfer," *IEEE Trans. Microw. Theory Techn.*, vol. 65, pp. 3409–3418, 2017.
- [23] J. H. Moon, J. J. Park, K.Y. Lee, and D. I. Kim, "Heterogeneously Reconfigurable Energy Harvester: An Algorithm for Optimal Reconfiguration," in *IEEE Int. of Thin. Jour.*, vol. 8, pp. 1437–1452, 2021.
- [24] W. Feller, *Introduction to probability theory and its applications*, Wiley, 3rd ed., 1968.
- [25] A. Georgiadis, G. V. Andia, and A. Collado, "Rectenna design and optimization using reciprocity theory and harmonic balance analysis for electromagnetic energy harvesting," *IEEE Ant. and Wirel. Prop. Lett.*, vol. 9, pp. 444–446, 2010.
- [26] H. Sun, Y. Guo, M. He, and Z. Zhong, "Design of a high-efficiency 2.45-ghz rectenna for low-input-power energy harvesting," *IEEE Ant. and Wirel. Prop. Lett.*, vol. 11, pp. 929–932, 2012.
- [27] C. R. Valenta and G. D. Durgin, "Harvesting wireless power: Survey of energy-harvester conversion efficiency in far-field, wireless power transfer systems," *IEEE Micr. Mag.*, vol. 15, pp. 108–120, June 2014.
- [28] B. Clerckx, R. Zhang, R. Schober, D. W. K. Ng, D. I. Kim, and H. V. Poor, "Fundamentals of wireless information and power transfer: From RF energy harvester models to signal and system designs," *IEEE J. Select. Areas Commun.*, vol. 37, pp. 4–33, Jan. 2019.
- [29] P. N. Alevizos, and A. Bletsas, "Sensitive and nonlinear far-field RF energy harvesting in wireless communications," *IEEE Trans. Wireless Commun.*, vol. 17, pp. 3670–3685, Jun. 2018.
- [30] L. Jing, E. De Carvalho, P. Popovski, and A. O. Martinez, "Design and performance analysis of noncoherent detection systems with massive receiver arrays," *IEEE Trans. Sign. Process.*, vol. 64, pp. 5000–5010, 2016.
- [31] R. Zhang, L. Yang, and L. Hanzo, "Energy pattern aided simultaneous wireless information and power transfer," *IEEE J. Select. Areas Commun.*, vol. 33, pp. 1492–1504, August 2015.
- [32] P. Liu, S. Gazor, Il-M. Kim, and D.I. Kim, "Noncoherent relaying in energy harvesting communication systems," *IEEE Trans. Commun.*, vol. 14, pp. 6940–6954, July 2015.
- [33] D. C. Daly, and A. P. Chandrakasan, "An energy-efficient OOK transceiver for wireless sensor networks," in *IEEE Journ. of Solid-State Circ.*, vol. 42, pp. 1003–1011, May 2007.
- [34] J. Tao, N. Wang, E. Jiaqiang Ng, Y. Zhu, and C.-H. Heng, "A 5-pJ/Bit OOK transmitter using MEMS-Based RF oscillator for IoT application in 180-nm CMOS," *IEEE Micr. and Wir. Compon. Let.*, vol. 31, pp. 1158–1161, Oct. 2021.
- [35] D. Papailiopoulos, G. A. Elkheir, and G. N. Karystinos, "Maximum-likelihood noncoherent PAM detection," *IEEE Trans. Commun.*, vol. 61, pp. 11521159, Mar. 2013.
- [36] M. Molefi, E. D. Markus, and A. Abu-Mahfouz, "Wireless power transfer for IoT devices - A review", *IEEE Int. Mult. Inf. Techn. and Eng. Conf. (IMITEC)*, Vanderbijlpark, S. Africa 2019.
- [37] A. Costanzo, D. Masotti, G. Paolini, and D. Schreurs, "Evolution of SWIPT for the IoT World: Near- and far-field solutions for simultaneous wireless information and power transfer," *IEEE Micr. Mag.*, vol. 22, pp. 48–59, Dec. 2021.
- [38] S. Shen, and B. Clerckx, "Joint waveform and beamforming optimization for MIMO wireless power transfer," *IEEE Trans. Commun.*, vol. 69, pp. 5441–5455, 2021.
- [39] E. Kwiatkowski, C. T. Rodenbeck, T. Barton, and Z. Popovic, "Power-combined rectenna array for X-band wireless power transfer," *IEEE MTT-S Intern. Micr. Symp. (IMS)*, L.A. USA, 2020.
- [40] X. Xu, A. Ozelikkale, T. McKelvey and M. Viberg, "Simultaneous information and power transfer under a non-linear RF energy harvesting model," in *Proc. IEEE Intern. Conf. Comm. Work.*, Paris, France, May 2017.
- [41] S. Bashir, S. Ali, S. Ahmed, and V. Kakkar, "Analog-to-digital converters: A comparative study and performance analysis," *Intern. Conf. on Comp., Commun. and Autom. (ICCCA)*, India, Jan. 2017.
- [42] O C. Ibe, *Markov processes for stochastic modeling*, Elsevier, 2nd ed., 2013.